

New physics above 50 TeV: probing its phenomenology through UHECR air-shower simulations

Stylianos Romanopoulos* and Vasiliki Pavliou†

*Department of Physics & Institute of Theoretical and Computational Physics,
University of Crete, GR-70013, Heraklion, Greece*

Institute of Astrophysics, Foundation for Research and Technology-Hellas, Vasilika Vouton, GR-70013 Heraklion, Greece

Theodore Tomaras‡

*Department of Physics & Institute of Theoretical and Computational Physics,
University of Crete, GR-70013, Heraklion, Greece*

(Dated: July 15, 2022)

Ground based observations appear to indicate that Ultra High Energy Cosmic Rays (UHECR) of the highest energies ($> 10^{18.7}$ eV) consist of heavy particles – shower depth and muon production data both pointing towards this conclusion. On the other hand, cosmic-ray arrival directions at energies $> 10^{18.9}$ eV exhibit a dipole anisotropy, which disfavors heavy composition, since higher-Z nuclei are strongly deflected by the Galactic magnetic field, suppressing anisotropy. This is the composition problem of UHECR. One solution could be the existence of yet-unknown effects in proton interactions at center-of-mass (CM) energies $\gtrsim 50$ TeV, which would alter the interaction cross section and the multiplicity of interaction products, mimicking heavy primaries. We study the impact of such changes on cosmic-ray observables using simulations of Extensive Air-Shower (EAS), in order to place constraints on the phenomenology of any new effects for high energy proton interactions that could be probed by $\sqrt{s} > 50$ TeV collisions. We simulate showers of primaries with energies in the range $10^{17} - 10^{20}$ eV using the CORSIKA code, modified to implement a possible increase in cross-section and multiplicity in hadronic collisions exceeding a CM energy threshold of 50 TeV. We study the composition-sensitive shower observables (shower depth, muons) as a function of cross-section, multiplicity, and primary energy. We find that in order to match the Auger shower depth measurements by means of new hadronic collision effects alone (if extragalactic UHECR are all protons even at the highest energies), the cross-section of proton-air interactions has to be ~ 800 mb at 140 TeV CM energy, accompanied by an increase of a factor of 2-3 in secondary particles. We also study the muon production of the showers in the same scenario. Although the muon production does increase, this increase is not enough to resolve the muon problem of UHECRs if the distribution of secondaries among different species remains unchanged with respect to the Standard Model prediction.

I. INTRODUCTION

Cosmic Rays (CR) are the most energetic particles in the universe. Over 100 years have passed since they were first discovered by Hess [1], yet still today their composition, origin and acceleration mechanism are subjects of debate. This lingering uncertainty stems not only from observational limitations but also from particle-physics uncertainties: the first collisions of ultra-high-energy cosmic rays (UHECRs $E \gtrsim 10^{18}$ eV) with the Earth's atmosphere occur at center-of-mass (CM) energies exceeding 40 TeV and reaching 300 TeV; for comparison, current lab tests of hadronic physics (in the Large Hadron Collider, LHC) only reach CM energies of 14 TeV.

Observationally, the greatest challenges in studying UHECRs are their low flux and their inability to penetrate the atmosphere: detection has to be indirect, tracing either the development of the extensive particle air

shower (EAS) caused by a CR's collision with the atmosphere, or the EAS products reaching the ground, or both; and dedicated UHECR observatories need collective areas of thousands of km^2 .

Despite significant progress in recent decades in improving statistics of UHECR detections thanks to very large facilities such as the Pierre Auger Observatory in Argentina [2] and the Telescope Array in the United States [3], important questions regarding UHECR astrophysics remain open. In particular, the distribution of UHECR arrival directions on the sky, their origin, and their composition constitute three persistent, interconnected puzzles.

Because cosmic rays are charged, it is not possible to directly associate their arrival directions with the sources that accelerate them. However, there are astrophysical arguments about possible classes and cosmic locations of cosmic-ray sources, with important implications for the resulting cosmic-ray properties.

At lower energies ($< 10^{12}$ eV), it is fairly certain that cosmic rays originate in Galactic sources. This is evidenced by differences in the cosmic ray fluxes estimated for different galaxies through observations of gamma rays originating in the decay of neutral pions pro-

* sromanop@physics.uoc.gr

† pavlidou@physics.uoc.gr

‡ deceased

duced through collisions of cosmic rays with interstellar gas (e.g., [4–6]). At very high energies ($> 8 \times 10^{18}$ eV) we are equally confident that cosmic rays are extragalactic, since the anisotropic distribution of arrival directions that starts emerging at these energies is not correlated with the Galactic plane or the Galactic center [7].

The exact energy at which the transition from Galactic to extragalactic cosmic rays occurs is still under debate (see, e.g., [8] for a recent review), however most recent works assume that it happens somewhere between 10^{17} and $10^{18.5}$ eV. Hints for this are seen both in the spectrum and in the composition of cosmic rays at this energy range. The steepening of the spectrum seen at the “second knee” and the transition, at the same energies, to a heavier composition [9] point towards a population originating in magnetically-confining accelerators reaching its maximum possible energy (as per the Hillas criterion, [10, 11]).

At energies between $\sim 10^{17}$ eV and $\sim 10^{18.5}$ eV, composition-sensitive observables from KASCADE-Grande, Auger, and Telescope Array indicate a transition back to lighter composition [12–14]. At $\sim 10^{18.7}$ eV the spectrum also becomes harder, a feature known as the ankle [14, 15]. There are two interpretations of the ankle. In the first, the ankle marks the transition to UHECR of extragalactic origin (e.g., [16–18]). In the second, this transition is assumed to have already happened at somewhat lower energies. As a result, the composition is already light at the ankle, and the ankle spectral feature is actually a “dip” caused by electron-positron losses (e.g., [19–21]).

The debate of ankle-versus-dip is not, however, the only controversy at these energies. A second one is the so-called composition problem of UHECR. This is summarized as follows: At energies of $10^{18.7}$ eV, composition-sensitive variables, taken at face-value, indicate a transition back to heavier composition [22]. However, there are certain astrophysical indicators *against* a heavy composition: (a) The spectrum at this energy is transitioning to a shallower slope, not a steeper one - i.e, there is no coincident spectral indication that the UHECR accelerators are reaching their maximum energy [23] (b) Anisotropies start to emerge at these energies [7, 24–27]. This might not be so severe a problem if the Galactic magnetic field has the overall low strengths indicated, e.g., by [28]. However, recent studies of the Galactic magnetic field have shown that it is approximately an order of magnitude stronger than previously thought [29] in a small region near the reported hotspot from TA [26, 27]. If indeed the average Galactic magnetic field is proven to be just a few times stronger than the existing models, combined with the dipole anisotropy at high energies, we can conclude that UHECR are light nuclei. The reason is that heavy nuclei are strongly deflected from Galactic magnetic fields and would spread over all the sky, eliminating all evidence of anisotropy. (c) Heavier nuclei photodissociate fast during propagation (e.g., [18, 30, 31]) – with the exception of iron – so the composition be-

comes lighter during propagation, unless it starts out as pure iron. However, iron is far from a best-fit to Auger composition-sensitive observables. Instead, observations can be better fit by a mix of intermediate-mass nuclei, requiring an astrophysically contrived composition of the accelerated particles at the source (e.g., [32–36]). In contrast, models that are more natural astrophysically are not in as good agreement with composition-sensitive observables [37, 38].

In addition to these astrophysical considerations, there are particle-physics considerations that add to the composition problem. Hybrid detectors such as Auger and Telescope Array measure composition indirectly, in two ways: from the atmospheric slant depth at which the shower reaches a maximum, X_{\max} (measured through fluorescent detectors); and from the number of muons reaching the ground (measured by surface array tanks). At a fixed primary CR energy, heavier nuclei will typically give a lower and less variable X_{\max} ; and they will produce more muons. The observations of X_{\max} and muon numbers are then compared against the predictions from air-shower simulations. However, the best-fit compositions from muons and X_{\max} do not match [39]: too many muons are produced on the ground compared to what would be expected from the best-fit composition obtained from X_{\max} alone.

The latter two problems indicate that the air-shower simulations (or rather, the hadronic collision simulation models on which these are based) may not be capturing correctly the development of showers. This is not altogether unexpected, since the first collision of a 10^{17} eV cosmic ray with a stationary atmospheric proton is already super-LHC: we are simulating collisions of these primaries with the atmosphere based on theoretical extrapolations of hadronic behavior to higher energies. This has led several authors to hypothesize that the problem may lie in the hadronic collision models themselves. The solution that has been proposed in this context is that, above a threshold energy E_{th} , the proton-Air interaction changes due to new physics beyond the SM. This scenario is widely recognized both by the Auger Collaboration [40–42] and other authors [43–46]. In this scenario, the composition of the primary remains light. In [46] (hereafter PT19) we calculated analytically phenomenological constraints on any new effect that would alter hadronic interactions in such a way as to mimic a heavy composition at the highest UHECR energies. We showed that if the multiplicity of first-collision products increased over the SM predictions at a certain rate, the growth of the average X_{\max} with energy can be fully explained while keeping the composition light even at the highest energies. We also showed that a simultaneous increase in the proton-air cross-section over the SM prediction would improve agreement of $\sigma_{X_{\max}}$ (the shower-to-shower variation in X_{\max}) with the data, although we did not calculate the optimal behavior of the cross-section to best match Auger observations.

In this paper, we extend the analytic formulation of

PT19 using EAS simulations. For that purpose, we use a widely known program: CORSIKA¹ [47]. CORSIKA uses extrapolations of SM at post-LHC energies to model hadronic interactions. In this work we used two such models: EPOS LHC [48] and QGSJETII-04 [49]. For low energy interactions we used FLUKA² [50] which is a Monte Carlo code used extensively at CERN. Our main goals are: (a) To test whether an increase in the multiplicity of first-collision products can indeed yield the changes in the X_{\max} distribution predicted in PT09 – as contrasted with, e.g. the implementation of such a change by [51], who found that the variance of X_{\max} remains practically unchanged under a change in product multiplicity. (b) To calculate the optimal change in cross-section that best matches Auger X_{\max} data. In contrast, in PT19 we did not fully explore the parameter space, but we only argued that an increase in cross section changes the X_{\max} variance in the direction of better agreement with Auger data. (c) To evaluate the impact of this scenario on the muon problem, which was not addressed in PT19.

This paper is organized as follows. In Section II we present the mathematical formulation of our implementation of new physics effects in the first collision of $E > 10^{18}$ eV CR with the atmosphere. We discuss the results of our simulations in Section III, and we summarize and discuss our conclusions in Section IV.

II. MATHEMATICAL FORMULATION

The “new physics above 50 TeV” scenario that we explore here using simulations of EAS implements two phenomenological changes in the *first collision* of the incoming primary cosmic ray with the atmosphere (as in PT2019): (1) an increase in the multiplicity of the first collision products; and (2) an increase in the cross section of the first interaction with the atmosphere. Our approach is phenomenological and not tied to any specific new physics model. However, several candidate particles and new physics mechanisms exist that might lead to such behavior (see, for example, [43, 52–54]).

In §II A we discuss how we describe quantitatively these phenomenological changes. We discuss how these changes impact the slant depth of the showers in §II B, and the muons reaching the ground in §II C. In §II D we describe how we implement the changes of §II A in air shower simulations using CORSIKA.

In this paper, we assume that all extragalactic cosmic rays reaching the Earth are protons. However, not all $E > 10^{18}$ eV cosmic rays detected on Earth are extragalactic, and, more importantly, the high-energy-end of the Galactic cosmic ray spectrum has a heavy composition, additionally affecting the slant depth and muon

	EPOS LHC	QGSJETII-04
σ_0 (mb)	527.61	499.35
β (mb)	49.95	37.49
X_0 (gr/cm ²)	707.38	692.03
α (gr/cm ²)	63.74	60.37

TABLE I. Parameters for cross section and shower maximum. These parameters were calculated by performing linear fit in the SM data from EAS simulation with proton as a projectile.

content. In order therefore to compare our results with observations, we additionally need a model for the way the Galactic cosmic ray flux cuts off with energy. We describe this model in §II E.

A. Parametrization of changes in cross section and multiplicity

The cross-section of protons with nitrogen has a logarithmic behaviour at high energies [55]. For that reason, the cross section is usually parameterized as

$$\sigma_{\text{p-Air}} = \sigma_0 + \beta \log \varepsilon \quad (1)$$

where σ_0 and β are constants. Here we normalize the energy scale as $\varepsilon = E/E_{\text{th}}$, where E_{th} is the threshold energy above which new physics sets in. Based on the arguments in PT2019, we will take $E_{\text{th}} = 10^{18}$ eV, corresponding, for a collision of an primary proton with a stationary atmospheric proton, to a CM collision energy of ~ 50 TeV. We note that this threshold is neither coincident with the location of the break seen in Auger X_{\max} data, nor fine-tuned (other choices that satisfy both that the threshold is ultra-LHC and that it lies below the Auger data break give similarly good results). We can calculate σ_0 and β from hadronic interaction models (here we use EPOS LHC and QGSJETII-04) and the standard-model extrapolations employed therein. The results are given in the first 2 lines of Table (I).

If new phenomena take place at $\varepsilon > 1$, the cross section of the first interaction may change. Here we assume that such a change will only affect the value of the coefficient β of the energy-dependent term, and that the cross section will be continuous at $\varepsilon = 1$:

$$\sigma_{\text{p-Air,new}} = \sigma_0 + \beta' \log \varepsilon \quad (2)$$

We will parameterize this change in terms of the fractional change δ in the coefficient β relative to its standard-model value. Defining then

$$\delta = (\beta' - \beta)/\beta, \quad (3)$$

we obtain

$$\sigma_{\text{p-Air,new}} = \sigma_{\text{p-Air}} + \delta \beta \log \varepsilon. \quad (4)$$

In other words, for $\varepsilon > 1$, the cross section will deviate logarithmically from its standard-model-predicted value

¹ CORSIKA version 7.7402

² FLUKA version 2020.0.3

at the particular energy, with a coefficient $\delta\beta$. Clearly, $\delta = 0$ corresponds to no change to the cross-section at any energy over the standard-model prediction. We note however that the uncertainty in the standard-model predictions for the proton-air cross-section to super-LHC energies is high (see, e.g., Fig. 2 of [51]), and values of δ as high as 3.5 could still be consistent with the standard model within uncertainties.

We also postulate an increase of the number of secondary particles produced after the first collision of the primary with the atmosphere. We limit the effect to the first collision since, for energies of interest, secondary particles will, with very high probability, have energies such that their collisions with air will occur at CM energies below the threshold for new physics. We parameterize this increase in first-collision product multiplicity by

$$n(\varepsilon) = N(\varepsilon)/N_{\text{SM}}(\varepsilon), \quad (5)$$

where N is the number of secondaries produced under new physics, and N_{SM} is the standard-model prediction for the number of secondaries. It is possible that new physics may also change the charged-particle ratio of the products; we do not however implement such a change here. We further discuss this issue in §III.

B. Shower maximum

The slant depth of the shower maximum is the air column density traversed by the EAS front – measured from the top of the atmosphere – for which the shower front achieves its maximum atmospheric ionization rate:

$$X_{\text{max}} = \int_{\infty}^{x_{\text{max}}} \rho(l) dl. \quad (6)$$

In Eq. (6), ρ is the density of the atmosphere, l is a length measured along the path the shower particles traverse in it, and x_{max} is the height of the shower maximum. X_{max} quantifies the total atmospheric column the shower has already encountered at its maximum, independently of the inclination of the incoming CR. X_{max} can be written as the sum of two terms. The first one is the column density after which the first interaction of the cosmic ray primary takes place, X_{int} ; and the second one is the column density between first interaction and shower maximum, X_{long} , corresponding to the “longitudinal” development of the shower:

$$X_{\text{max}} = X_{\text{int}} + X_{\text{long}}. \quad (7)$$

1. The first interaction: X_{int}

The probability that a CR has not interacted with the atmosphere in the vicinity of height x is

$$\exp\left(-\frac{\sigma_{\text{CR-Air}}}{m} \int_{\infty}^x \rho(l) dl\right),$$

where m is the average mass of the particles in the atmosphere (mainly nitrogen) and $\sigma_{\text{CR-Air}}$ is the cosmic-ray–air cross section for the energy of the primary. The average value of the depth of the first interaction for a given primary energy thus is

$$\langle X_{\text{int}} \rangle = \frac{m}{\sigma_{\text{CR-Air}}(\varepsilon)}. \quad (8)$$

Since X_{int} follows Poisson statistics, its variance will be

$$\text{Var}(X_{\text{int}}) = \langle X_{\text{int}} \rangle^2 = \frac{m^2}{\sigma_{\text{CR-Air}}^2(\varepsilon)}. \quad (9)$$

If new physics sets in for $\varepsilon > 1$, the distribution of X_{int} for primaries of a given energy will be affected through the change in $\sigma_{\text{CR-Air}}$, which (assuming the composition remains light) will take the value of $\sigma_{\text{p,Air,new}}$ given by Eq. (4):

$$\langle X_{\text{int,new}} \rangle = \frac{m}{\sigma_{\text{p-Air}}(\varepsilon) + \delta\beta \log \varepsilon}, \quad (10)$$

and

$$\text{Var}(X_{\text{int,new}}) = \frac{m^2}{[\sigma_{\text{p-Air}}(\varepsilon) + \delta\beta \log \varepsilon]^2}. \quad (11)$$

2. The longitudinal development: X_{long}

Following the CR interaction with the atmosphere, secondary and subsequent generation of particles are produced. As the shower of particles evolve through the atmosphere, the energy per particle decreases, partly because of ionization losses and partly because of new particle production. This process continues until the energy of the shower particles drops below the energy threshold of new particle production, at which point the shower continues to evolve by ionization losses alone. This evolution of the shower is observable through the fluorescence of ionized atoms of the atmosphere, which can be detected with ground telescopes. The intensity of this fluorescent light encodes the energy loss rate of the shower front. X_{long} measures the column density traversed by the shower front *after the first interaction* until the energy loss rate reaches its maximum value.

The dependence of the longitudinal column, X_{long} , with energy can be derived from the simple model of Heitler [56, 57], where the initial particle produces two daughter particles which split the primary’s energy, and

the process continues until the energy of each particle reaches a critical energy below which the process cannot continue.

This results to a logarithmic increase of X_{long} with energy. A more realistic calculation of X_{long} is more complex because additional phenomena take place (e.g. bremsstrahlung, pair production, pion production, hadronization), and there are significant shower-to-shower fluctuations. For that purpose numerical simulations are used to follow the development of EAS (e.g. CORSIKA). The final behavior of $\langle X_{\text{long}} \rangle$ with energy, however, is still logarithmic:

$$\langle X_{\text{long}} \rangle = X_0 + \alpha \log \varepsilon \quad (12)$$

where X_0 and α are constants, while $\sigma_{X_{\text{long}}}$ remains approximately constant with energy.

In the last 2 lines of Table (I) we show the best-fit parameters X_0 and α for protons, derived from CORSIKA EAS simulations using two different models (EPOS LHC and QGSJETII-4) of hadronic interactions. Both models employ standard-model extrapolations for collisions at super-LHC energies. The parameters do depend slightly on the hadronic interactions model, however both models produce qualitatively similar results.

If now new physics sets in for $\varepsilon > 1$, the distribution of X_{long} will change. To quantify this change, we model empirically the shower as $n(\epsilon)$ "component showers", of energy $\epsilon/n(\epsilon)$ on average, developing independently. Note that this approach is conceptually and qualitatively different from that of [51] who used a multiplicative factor to increase the number of products in each collision - the most prominent difference being that the presence of independently developing "component showers" decreases the shower-to-shower fluctuations of X_{long} (i.e. $\sigma_{X_{\text{long}}}$), while a multiplicative increase of products of identical distribution as the original shower leaves $\sigma_{X_{\text{long}}}$ unchanged.

Under this change, $\langle X_{\text{long,new}} \rangle$ becomes [from Eq. (12)]

$$\langle X_{\text{long,new}} \rangle = X_0 + \alpha \log \frac{\varepsilon}{n(\epsilon)}. \quad (13)$$

To produce an analytical estimate the variance of X_{long} we take, as in PT19, the average of individual "component-shower" longitudinal depth, $\frac{1}{n} \sum_i X_{\text{long},i}$ to be a reasonable estimation of X_{long} . Then X_{long} is the "sample mean" of n "draws" from the underlying distribution of $X_{\text{long},i}$ and the distribution of these "sample means" has a variance that is given by the "error in the mean" formula,

$$\text{Var}(X_{\text{long,new}}) = \frac{\text{Var}(X_{\text{long},i})}{n(\varepsilon)}. \quad (14)$$

Here $\text{Var}(X_{\text{long},i})$ is the variance of $X_{\text{long},i}$, and it can be assumed to follow the SM predictions, since each sub-shower of the sample will have $\epsilon < 1$.

3. New physics mimics a transition to heavy composition

The average value and the variance of X_{max} are sensitive to the first interaction - both its cross-section and the multiplicity of its products. A higher first-interaction cross-section will result to lower $\langle X_{\text{int}} \rangle$ and $\text{Var}(X_{\text{int}})$, and therefore lower $\langle X_{\text{max}} \rangle$. A large number of first collision products will distribute the energy of the primary more widely, resulting to lower $\langle X_{\text{long}} \rangle$ and therefore to lower $\langle X_{\text{max}} \rangle$. A larger number of first-collision products will also result to reduced shower-to-shower fluctuations in X_{long} and in turn to a lower $\text{Var}(X_{\text{long}})$ and a lower $\text{Var}(X_{\text{max}})$.

A heavy primary composition will drive both $\langle X_{\text{max}} \rangle$ and $\text{Var}(X_{\text{max}})$ to lower values for a given energy, through both an increased cross-section of the primary-air collision, and an increased first-collision product multiplicity. The new-physics scenario we discuss here will also move the X_{max} distribution in the same direction through similar changes in cross-section and multiplicity, and can thus mimic a transition to a heavier composition.

4. Constraining $n(\varepsilon)$ and δ

The empirical model we have presented here features a *free parameter* δ and a *free function* $n(\varepsilon)$. However, if we assume that the change of slope in $\langle X_{\text{max}}(\epsilon) \rangle$ observed by Auger at the highest energies is, *in its entirety*, due to new physics, so that all primaries at these energies are protons, we can completely determine $n(\epsilon)$ as a function of δ , leaving only a single free parameter in our model (which can also be optimized by comparison to other moments of the X_{max} distribution, as we will see in §III).

The Auger Collaboration reports, for energies $E \geq 10^{18.3}$ eV

$$\langle X_{\text{max,Auger}} \rangle = X_{0,\text{Auger}} + \alpha_{\text{Auger}} \log \varepsilon \quad (15)$$

with $X_{0,\text{Auger}} = 749.74$ gr/cm² and $\alpha_{\text{Auger}} = 23.98$ gr/cm². Simulated data of pure protons air showers indicate a difference from Auger observations above this energy. By equating the behaviour of Auger data to the results of the postulated new physics effects at $\epsilon > 1$ [using Eqs. (7), (10), and (13)] we obtain

$$\langle X_{\text{max,Auger}} \rangle(\varepsilon) = \frac{m}{\sigma_{\text{p-Air}}(\varepsilon) + \delta \beta \log \varepsilon} + X_0 + \alpha \log \frac{\varepsilon}{n(\varepsilon)} \quad (16)$$

and solving for the multiplicity we obtain

$$\log n(\varepsilon) = \frac{X_0 - X_{0,\text{Auger}}}{\alpha} + \frac{\alpha - \alpha_{\text{Auger}}}{\alpha} \log \varepsilon + \frac{1}{\alpha \sigma_{\text{p-Air}}(\varepsilon) + \delta \beta \log \varepsilon} m \quad (17)$$

with $\sigma_{\text{p-Air}}(\varepsilon)$ given by Eq.(1).

The variance of X_{max} under new physics effects can be estimated through

$$\text{Var}(X_{\text{max,new}}) = \text{Var}(X_{\text{int,new}}) + \text{Var}(X_{\text{long,new}}) \quad (18)$$

using Eqs. (11) and (14), yielding

$$\begin{aligned} \text{Var}(X_{\text{max,new}}) &= \sigma_{X_{\text{max}}}^2 \\ &= \frac{m^2}{[\sigma_{\text{p-Air}}(\varepsilon) + \delta \beta \log \varepsilon]^2} + \frac{\text{Var}(X_{\text{long}})}{n(\varepsilon)}, \end{aligned} \quad (19)$$

which again has only one free parameter: δ . Clearly, δ can be optimized by comparing Eq. (19) with Auger data on $\sigma_{X_{\text{max}}}$.

C. Muons

The muonic part of EAS is also a problem in UHECR physics. Muons are produced mainly when charged pions or kaons decay, indicating hadronic interactions. They have a large mean free path and consequently their journey in the atmosphere is mostly undisturbed. Upon reaching the ground, muons can be detected via the Cherenkov radiation they produce inside the water tanks comprising the surface array of hybrid experiments such as Auger and TA. Thus the energy and spacial distribution of muons can be measured.

A useful parameter used to compare experiment with simulations is the ratio

$$R_\mu = \frac{N_\mu}{N_{\mu,19}} \quad (20)$$

where N_μ is the number of muons detected on the ground. The reference parameter $N_{\mu,19} = 2.148 \cdot 10^7$ is inferred from simulations assuming proton as the primary particle with energy of 10^{19} eV, taking into consideration the detector's response for muons above 0.3 GeV^3 that reach Auger's site at an altitude of 1425 m with inclination of $\theta = 60^\circ$. Aab *et al.* [58] report that $N_{\mu,19}$ does not depend strongly on the selected high energy model. They quote a $\sim 11\%$ systematic error introduced in this way. The reason for selecting so inclined showers is because for inclination $\theta > 60$, EAS are dominated mostly by muons, since the electromagnetic part is absorbed by the atmosphere. This is in fact the inclination we used in our simulations.

Auger reports that the average of that ratio depends on energy as

$$\langle R_\mu \rangle = a \left(\frac{E}{10^{19} \text{ eV}} \right)^b \quad (21)$$

where $a = 1.841$ and $b = 1.029$. They also report a relative standard deviation of

$$\sigma[R_\mu]/\langle R_\mu \rangle = 0.136. \quad (22)$$

Auger observes 25 – 40% more muons at 10^{19} eV than high energy models predict, assuming proton as a primary. However, muons are observed to be in overabundance *even if a heavier composition, consistent with the one that would produce the observed $\langle X_{\text{max}} \rangle(\epsilon)$ is assumed for the primaries.*

In the scenario where proton interactions change above 10^{18} eV introducing new physics, the muon production will change due to the increase of multiplicity for the secondary particles.

The total number of muons on the ground will be the sum of muons that each component-shower produces. Note that each component-shower does not produce the same amount of muons.

We then expect the average number of muons on the ground to be

$$\langle N_{\mu, \text{new}}(\varepsilon) \rangle = n(\varepsilon) \langle N_\mu(\varepsilon/n) \rangle. \quad (23)$$

D. CORSIKA simulations

We now turn to EAS simulations. We wish to: (a) test whether the implementation, in simulations, of new physics as discussed in §II A will produce the same behavior as our analytic approximations; and (b) determine the optimal phenomenological parametrization (cross section and the multiplicity, quantified by δ and $n(\varepsilon)$ in our description) that any new proton-air interaction must exhibit in order for EAS to produce the observed data in Auger if the composition of primaries is to remain light up to the highest energies.

We simulated showers induced by primaries with energies in the range $10^{17} - 10^{20}$ eV with step in $\log E$ of 0.1. At each energy bin, we performed 1000 EAS simulations. We simulated EAS with the first collision treated either with SM extrapolations, or with new physics as per our phenomenological implementation. We performed SM EAS simulations for proton primaries with $E < E_{\text{th}} = 10^{18}$ eV, and for the heavier Galactic primaries (see next section), since their per-nucleon kinetic energy never exceeds 10^{18} eV. We implemented new physics for all proton primaries with $E > 10^{18}$ eV.

CORSIKA EAS simulations using either EPOS-LHC or QGSJETII-04 yielded our SM results. For low-energy interactions we used FLUKA. We also used the CONEX hybrid scheme [59] which decreases the simulation time dramatically. Each simulation generates three output files. The first records the energy deposited as a function of depth in the atmosphere. We fitted a Geisser-Hillas

³ This is the Cherenkov threshold for Auger's water tanks.

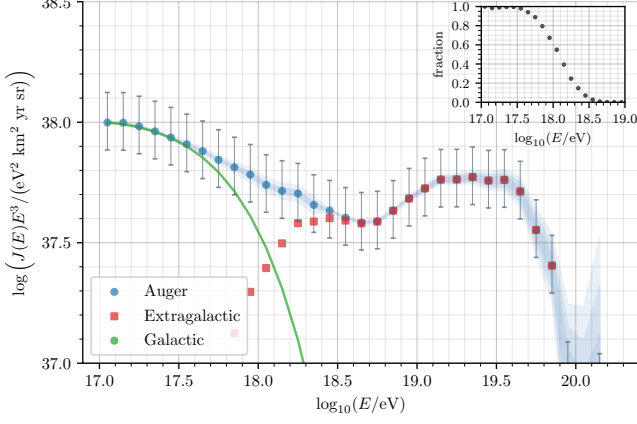


FIG. 1. CR energy spectrum (flattened by E^3). Blue: Auger Collaboration data. Green: Galactic CR flux model, assuming power law at low energies with an exponential cutoff at $10^{17.9}$ eV. Red: extragalactic CR flux, obtained as the difference between observed data and Galactic CR. Inset: fraction of Galactic to total CR flux

function

$$\frac{dE}{dX}(X) = N_{max} \left(\frac{X - W_0}{X_{long} - W_0} \right)^{\frac{X_{long} - W_0}{\lambda}} \times \exp \left(\frac{X_{long} - X}{\lambda} \right) \quad (24)$$

to the simulated data to estimate the shower longitudinal-development maximum, X_{long} , for each shower. For each energy bin, we then calculated the average value of X_{long} and its variance.

The second output file records information on the cross section of the primary with the atmosphere and from it we calculated $\langle X_{int} \rangle$. The second output file also contains the number of muons detected on the ground. We fitted a convolution of a Gaussian with an exponential to calculate the average value and the relevant variance of the number of muons on the ground. The third output file (stack file) contains information about the secondary particles produced after the first interaction. The results from this run are the Standard Model predictions from extrapolated models.

For the new-physics simulations, we used the following approach. For a given value of δ , we first calculated the multiplicity according to Eq.(17) at each energy bin. We then combined stack files from the same energy bin (produced by SM simulations) according to the calculated multiplicity: we rounded $n(\epsilon)$ to the nearest integer, and we combined as many stack files, accounting for energy and momentum conservation. To this end, we divided the energy and momentum of each particle by the number of stacked files. We then used the combined stack files as input to CORSIKA and continued the simulation of the EAS, obtaining data files for the energy deposition

as a function of depth in the atmosphere and the muon number on the ground. The cross section was calculated from Eq.(2).

E. Cosmic Ray Flux

At energies above $10^{18.3}$ eV, both Auger and TA observe a dipole distribution of CR uncorrelated with the galactic plane [60, 61]. This indicates that above this energy, CR are of extra-galactic origin. The energy at which this transition takes place is an important input for our calculations. The reason is that Galactic CR are heavy particles and thus the energy per nucleon will be below the threshold of new physics. As a result we need not apply any new physics corrections to their EAS simulations.

We model this transition using a simple, phenomenological approach, based on three assumptions: (1) That above 10^{17} eV cosmic rays consist of a single, fixed-composition Galactic component, and a single, fixed-composition extragalactic component. The energy-dependent fraction of Galactic CR is $f(\epsilon)$. The fraction of extragalactic CR is then $1 - f(\epsilon)$. (2) That above 10^{17} eV we can model the Galactic CR spectrum (differential particle flux $J(\epsilon)$) as a power law of slope $-\gamma_G$, cutting off exponentially at a characteristic energy ϵ_G , corresponding to the maximum energy of Galactic CR accelerators:

$$J_G(\epsilon) = J_{G,0} \left(\frac{\epsilon}{\epsilon_{17.5}} \right)^{-\gamma_G} \exp \left(-\epsilon/\epsilon_G \right) \quad (25)$$

where $\epsilon_{17.5} = 10^{17.5} \text{ eV}/E_{th} = 10^{-0.5}$. (3) That CR at energies lower than those where losses (either e^+e^- or pion photoproduction) become important, the extragalactic CR flux $J_{EG}(\epsilon)$ is a single power law.

At low energies ($E < 10^{17.5}$ eV), Auger data constrain $J_{G,0} = 4.1 \times 10^{-15} (\text{km}^2 \text{ eV yr sr})^{-1}$, and $\gamma_G = 2.9$. By virtue of our third assumption above, we can also constrain ϵ_G by demanding that, for $10^{17.5} \text{ eV}/E_{th} < \epsilon < 10^{18.2} \text{ eV}/E_{th}$ the extragalactic spectrum $J_{EG}(\epsilon) = J_{total, Auger} - J_G(\epsilon)$ is consistent with a single power law. We thus find $\epsilon_G = 10^{17.9} \text{ eV}/E_{th}$, which results in an extragalactic spectrum consistent with $J_{EG}(\epsilon) \propto \epsilon^{-2.0}$ between $10^{17.5}$ and $10^{18.2}$ eV (see Fig. 1).

The resulting Galactic CR fraction, $f(\epsilon) = J_G(\epsilon)/J_{total, Auger}(\epsilon)$ is shown in the inset of Fig. 1. We note that under the three assumptions adopted here, extragalactic CR are found to dominate already at 10^{18} eV, the composition at $10^{18.5}$ is light, and the ankle must be an e^+e^- "dip". In this simple scenario, the probability density function of X_{max} will be

$$p(X_{max}) = f p_G(X_{max}) + (1 - f) p_{EG}(X_{max}) \quad (26)$$

leading to an average shower maximum

$$\langle X_{max} \rangle = f \langle X_{max} \rangle_G + (1 - f) \langle X_{max} \rangle_{EG} \quad (27)$$

and its variance

$$\begin{aligned} \text{Var}(X_{\text{max}}) &= f \text{Var}(X_{\text{max,G}}) \\ &+ (1 - f) \text{Var}(X_{\text{max,EG}}) \\ &+ f(1 - f) (\langle X_{\text{max}} \rangle_G - \langle X_{\text{max}} \rangle_{EG})^2 \end{aligned} \quad (28)$$

with subscripts G and EG referring to the Galactic and extragalactic populations respectively.

At energies around 10^{17} eV, CR are mainly of Galactic origin. In this paper we assume Galactic CR to be one type of nucleus for simplicity. We assume the Galactic component to be helium for simplicity – lighter than PT09, who had assumed carbon. Ultimately, the Galactic component should ideally be simulated with appropriate mixed composition, with each species cutting off at different energies according to its charged, as per the Hillas criterion [10].

III. RESULTS

We performed CORSIKA simulations as described in §IID for $\delta = 0, 2.9, 3.5, 4, 6, 8$ and 10, treating the Galactic-to-extragalactic transition as described in §IIE. The simulation results for $\langle X_{\text{max}} \rangle$ are (by construction) in excellent agreement with Auger data⁴ for all values of δ (Fig. 2). Our simulations are also a much improved fit to the $\sigma_{x_{\text{max}}}$ data even for $\delta = 0$ (no change in cross section, only multiplicity increases). For higher δ the agreement improves further and is optimal for δ between 4 and 8 (Fig. 3). In Figs. 2 and 3 we did not plot results for all simulated values of δ in order to keep the figures legible.

Figs. 2 and 3 show a deviation of the simulation results from observations at low energies. We expect that this discrepancy is due to the assumption of a Galactic component consisting purely of helium. A more reasonable assumption is a mixture of helium, carbon and oxygen, with ratios that depend on the energy. However, since the details of Galactic CR composition have little to no impact on the (dis)agreement between theory and observations of X_{max} at the highest energies, we chose, for simplicity, not to focus on the modeling of the Galactic component in this work. Instead, we implement the very simple recipe described above aiming only to show the direction in which $\langle X_{\text{max}} \rangle$ and $\sigma_{X_{\text{max}}}$ will change due to the Galactic-to-extragalactic transition. We plan to return to this problem and relax the assumption of a single-species Galactic component in a future publication.

We next explore the agreement between new-physics $\sigma(X_{\text{max}})$ and observed Auger data, quantifying it by means of the reduced χ^2 statistic. Since we have treated the Galactic component in a very approximate way, we

⁴ Throughout this paper, we use error bars for systematic uncertainties, and shaded areas to indicate 1, 2, and 3 σ statistical uncertainties.

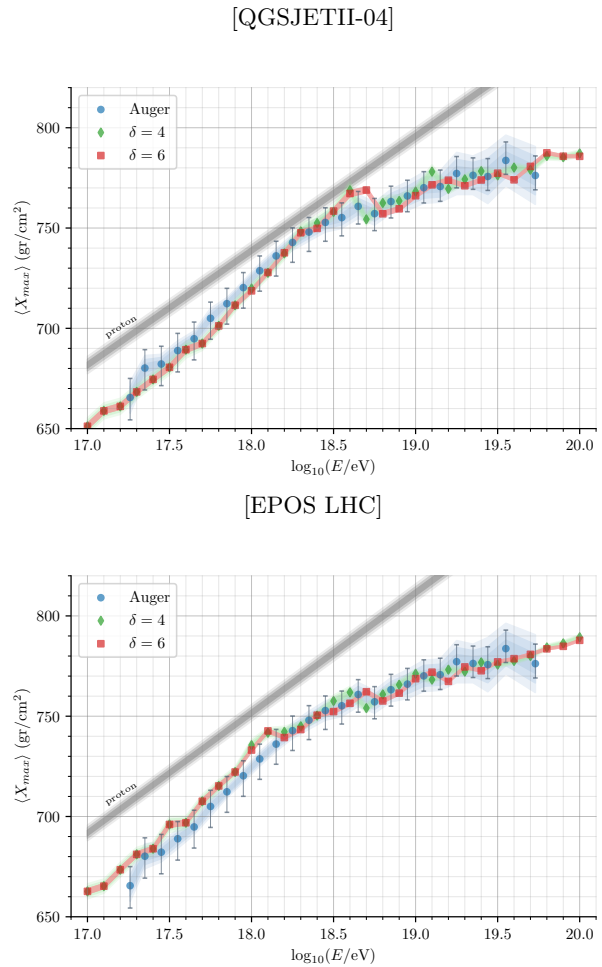
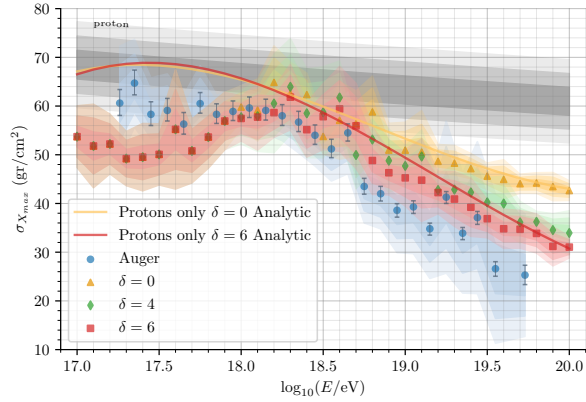


FIG. 2. Average shower maximum as a function of energy. Standard model extrapolations (grey) through QGSJETII-04 (upper) and EPOS LHC (lower) do not agree with observations from Auger Observatory (blue) above $E_{\text{th}} = 10^{18.5}$ GeV. When we alter the way the cross section and the first-interaction product multiplicity scale with energy as in Eqs. (4) and (17), EAS simulations with protons as a primaries (green and red) reproduce the observed data well at the highest energies. The simplifying assumption of a single component Galactic CR is the reason our simulations deviate from observational data at lower energies.

only use energies at which extragalactic protons have fully dominated the UHECR flux ($E > 10^{18.5}$ eV) for this comparison. In Fig.(4) we plot the reduced χ^2 as a function of δ for our EAS simulation results (datapoints), as well as for our analytic approximation for $\sigma_{X_{\text{max}}}$ given by Eq. (19) (solid lines). We calculate the position of minimum χ^2 for our simulations by fitting parabolas (dashed lines) to our datapoints. EPOS-LHC has a minimum of $\chi^2 = 1.5$ at $\delta = 4.8$ and QGSJETII-04 has a minimum of $\chi^2 = 5.2$ at $\delta = 6.7$. EPOS-LHC has overall better performance. At their minimum χ^2 the cross section at an energy of 10^{19} GV rises to 830 mb (788 mb) for EPOS-LHC (QGSJETII-04). Furthermore at the same energy

[QGSJETII-04]



[EPOS LHC]

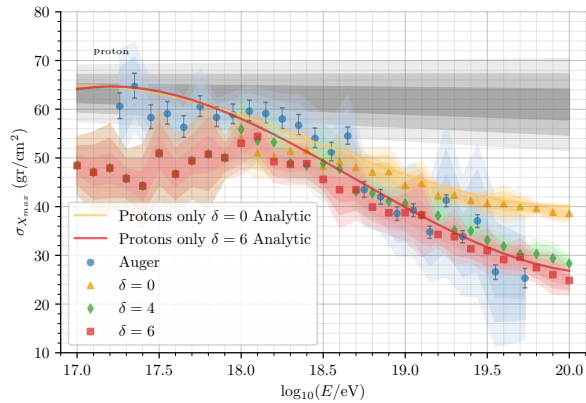


FIG. 3. Standard deviation of shower maxima as a function of energy. Although the mean of X_{\max} does not depend on the parameter δ (see Fig. 2), its standard deviation does. We obtain the best agreement between simulated $\sigma_{X_{\max}}$ and Auger observations for δ near 6 for QGSJETII-04 (upper) and for δ near 4 for EPOS-LHC (lower). Further increment of the δ parameter does not result in significant changes at high energies, as $\sigma_{X_{\max}}$ quickly reaches an asymptotic behavior.

the multiplicity has increased by a factor of 3 (2).

In Figs. 5 and 6 we show how the changes in cross-section and multiplicity in our scenario affect the number of muons measured on the ground. Fig. 5 shows the fractional difference of muons on the ground from simulations relative to the data observed by Auger. The new-physics scenario produces more muons than the SM prediction. Although this is an improvement, still a deviation between 30 – 37% from observational data persists. The reason is that the muon production does not depend strongly on the overall multiplicity of the secondary particles but rather on the ratio of pions and kaons produced after the first interaction [62]. The fraction of such particles in the products of the first collision does not change in the implementation of new physics we have considered here. However, such a change in

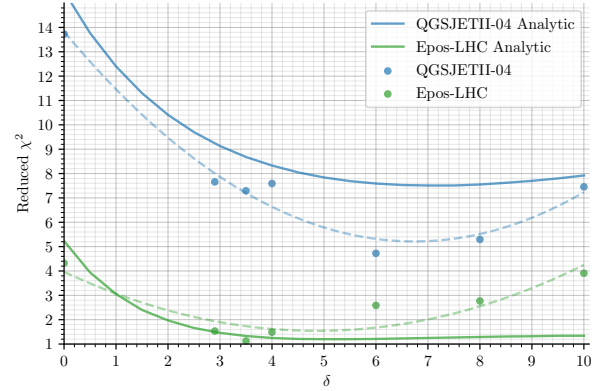


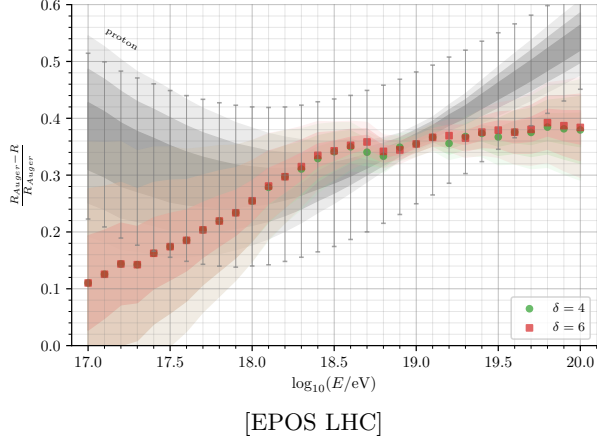
FIG. 4. Agreement between new-physics EAS simulations and Auger data for $\sigma_{X_{\max}}$ and $E > 10^{18.5}$ eV, quantified through the reduced χ^2 statistic, as a function of the value of the δ parameter. Overall, EPOS-LHC simulations produce results more consistent with observational data. To find the position of the minimum χ^2 , we perform a parabolic fit to the datapoints. The locations of the minima are at $\delta = 4.8$ for EPOS-LHC and at $\delta = 6.7$ for QGSJETII-04.

the charged-particle ratio may be an important feature in any specific new-physics model that attempts to fully explain the UHECR composition problem, including the muon problem. We do however point out that the residual discrepancy between simulated and observed number of muons in our current implementation is constant with energy, unlike the SM predictions, where the discrepancy increases with energy. Our implementation additionally produces a *variance* for the muon number that is consistent with observed data (Fig.6), including the correct trend with energy. We plan to revisit this issue in a future publication, adding the possibility of a change in the charged-particle ratio.

IV. SUMMARY AND CONCLUSIONS

We performed simulations of EAS with CORSIKA, appropriately modified for interactions above $E_{\text{th}} = 10^{18}$ eV to feature an increased proton-air cross-section and first-collision product multiplicity. We have parameterized the increase in cross section through a parameter δ , defined as the fractional increase of the coefficient of logarithmic growth with energy of the proton-air cross-section with respect to its standard-model value (see Eq. 4). We have parameterized the increase in product multiplicity through a function $n(\varepsilon)$, defined as the ratio of first-collision products over their SM-predicted number. By demanding that Auger observations of $\langle X_{\max} \rangle$ as a function of energy above $10^{18.7}$ eV are reproduced under the assumption that all UHECR at these energies are protons, we can determine $n(\varepsilon)$ for any given value of δ (see Eq. 17). This then leaves δ as the only parameter

[QGSJETII-04]



[EPOS LHC]

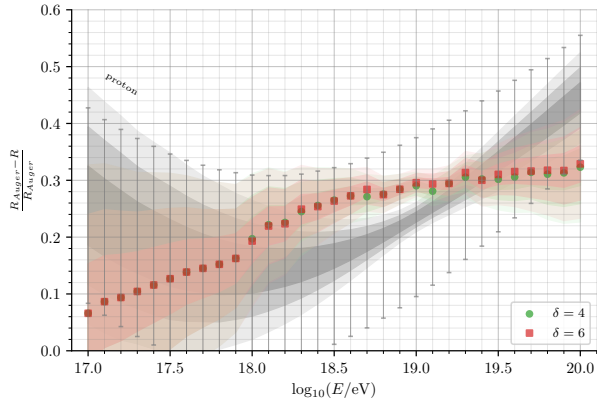


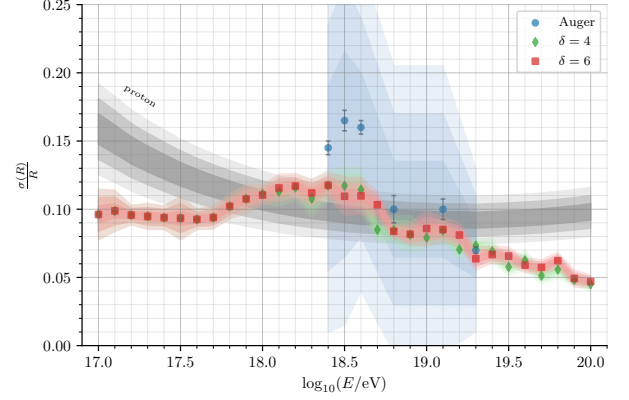
FIG. 5. Fractional difference of muons on the ground predicted by simulations relative to the observed data at the Auger Observatory. When new physics sets in above E_{th} , the number of muons change (green and red), due to the change in product multiplicity (hence, independently of δ). This change does not fully reconcile the simulated number of muons with observations. However, unlike the SM prediction (grey), the discrepancy does not increase with energy above $10^{18.5}$ eV, but rather stabilizes around 30% (40%) for EPOS-LHC (QGSJETII-04).

in our description.

We have shown that these modifications to hadronic interactions at energies above 10^{18} eV are sufficient to reproduce observations of X_{max} . The growth of $\langle X_{max} \rangle$ is reproduced for any value of δ (by construction), and $\sigma_{X_{max}}$ is best reproduced for δ between 4 and 7. If QGSJETII-04 is used for SM modeling of high-energy hadronic interactions, the optimal value for δ is 6.7. For EPOS-LHC, the optimal value for δ is 4.8. Epos-LHC with $\delta = 4.8$ provides the best overall fit to Auger X_{max} data at $E > 10^{18.5}$ eV. In each case, product multiplicity increases by a factor $n(\varepsilon)$ given by Eq. (17).

These results provide phenomenological constraints on the properties (cross section, multiplicity) of any new

[QGSJETII-04]



[EPOS LHC]

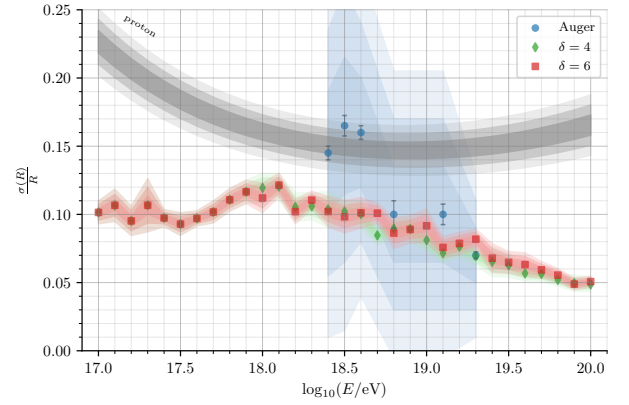


FIG. 6. Standard deviation over average of the muon ratio as a function of energy. When new physics sets in above E_{th} , this quantity becomes more consistent with observed data than SM predictions (grey), and reproduces the trend with energy observed by Auger.

effect beyond the SM that may set it for collisions at CM energies exceeding ~ 50 TeV, if such an effect is to be held responsible for the change of behavior of the X_{max} distribution observed by Auger for collisions of primaries more energetic than $10^{18.7}$ eV with the atmosphere.

As far as the muon problem is concerned, we found that although the change in multiplicity we have investigated here does improve the agreement between Auger data and EAS simulations, it is not by itself sufficient to fully resolve the discrepancy. For this reason, we speculate that any new effect setting in at 50 TeV may also induce a change in the charged-particle ratio, which would further increase the number of muons produced and detected on the ground. We plan to investigate this possibility in a future publication.

Current and planned advances in the tomographic mapping of the Galactic magnetic field through local measurements [29, 63–67] are expected to make feasible an electromagnetic determination of the charge of

UHECR of the highest energies in the near future [68]. If such studies provide unequivocal evidence that UHECR at the highest energies are indeed protons, then this will be a strong argument in favor of new physics setting in for hadronic interactions at CM energies above 50 TeV, with the phenomenology of any such new effect exhibiting the behavior calculated in this work.

ACKNOWLEDGMENTS

S.R. and V.P. would like to dedicate this work to the memory of our friend and collaborator Theodore Tomaras whom we have lost way too soon. We will always fondly remember all the exciting and fruitful scientific discussions and debates that we have had and

we will be sorely missing the ones that will now never take place. We thank Alan Watson, Nicusor Arsene, Konstantina Dolapsaki, Andreas Tersenov, and Christos Litos for helpful comments and discussions that improved this manuscript, and Dieter Heck for valuable feedback on the use of CORSIKA. This work was supported by the Hellenic Foundation for Research and Innovation (H.F.R.I.) under the “First Call for H.F.R.I. Research Projects to support Faculty members and Researchers and the procurement of high-cost research equipment grant” (Project 1552 CIRCE). V.P. acknowledges support from the Foundation of Research and Technology - Hellas Synergy Grants Program through project MagMASim, jointly implemented by the Institute of Astrophysics and the Institute of Applied and Computational Mathematics.

-
- [1] V. F. Hess, Über Beobachtungen der durchdringenden Strahlung bei sieben Freiballonfahrten, *Phys. Z.* **13**, 1084 (1912).
 - [2] J. Abraham and *et al*, Properties and performance of the prototype instrument for the Pierre Auger Observatory, *Nuclear Instruments and Methods in Physics Research A* **523**, 50 (2004).
 - [3] T. Abu-Zayyad and *et al*, The surface detector array of the Telescope Array experiment, *Nuclear Instruments and Methods in Physics Research A* **689**, 87 (2012), arXiv:1201.4964 [astro-ph.IM].
 - [4] P. Sreekumar and *et al*, Constraints on the cosmic rays in the Small Magellanic Cloud, *Phys. Rev. Lett.* **70**, 127 (1993).
 - [5] M. Ackermann and *et al*, Deep view of the Large Magellanic Cloud with six years of Fermi-LAT observations, *aap* **586**, A71 (2016), arXiv:1509.06903 [astro-ph.HE].
 - [6] M. Ackermann and *et al*, Observations of M31 and M33 with the Fermi Large Area Telescope: A Galactic Center Excess in Andromeda?, *apj* **836**, 208 (2017), arXiv:1702.08602 [astro-ph.HE].
 - [7] A. Pierre Auger Collaboration, Aab and *et al*, Observation of a large-scale anisotropy in the arrival directions of cosmic rays above 8×10^{18} eV, *Science* **357**, 1266 (2017), arXiv:1709.07321 [astro-ph.HE].
 - [8] S. Gabici, C. Evoli, D. Gaggero, P. Lipari, P. Mertsch, E. Orlando, A. Strong, and A. Vittino, The origin of Galactic cosmic rays: Challenges to the standard paradigm, *International Journal of Modern Physics D* **28**, 1930022-339 (2019), arXiv:1903.11584 [astro-ph.HE].
 - [9] A. Chiavassa and *et al*, Summary of the main results of the KASCADE and KASCADE-Grande experiments, in *European Physical Journal Web of Conferences*, European Physical Journal Web of Conferences, Vol. 208 (2019) p. 03002.
 - [10] A. M. Hillas, The Origin of Ultra-High-Energy Cosmic Rays, *araa* **22**, 425 (1984).
 - [11] K. Kotera and A. V. Olinto, The Astrophysics of Ultrahigh-Energy Cosmic Rays, *araa* **49**, 119 (2011), arXiv:1101.4256 [astro-ph.HE].
 - [12] A. Aab *et al.* (Pierre Auger), Combined fit of spectrum and composition data as measured by the Pierre Auger Observatory, *JCAP* **04**, 038, [Erratum: *JCAP* 03, E02 (2018)], arXiv:1612.07155 [astro-ph.HE].
 - [13] Haungs, A., Apel, W.D., Arteaga-Velázquez, J.C., Bekk, K., Bertaina, M., Blümer, J., Bozdog, H., Brancus, I.M., Cantoni, E., Chiavassa, A., Cossavella, F., Daumiller, K., Souza, V. de, Pierro, F. Di, Doll, P., Engel, R., Fuhrmann, D., Gherghel-Lascu, A., Gils, H.J., Glasstetter, R., Grupen, C., Heck, D., Hörandel, J.R., Huege, T., Kampert, K.-H., Kang, D., Klages, H.O., Link, K., Luczak, P., Mathes, H.J., Mayer, H.J., Milke, J., Mitrica, B., Morello, C., Oehlschläger, J., Ostapchenko, S., Pierog, T., Rebel, H., Roth, M., Schieler, H., Schoo, S., Schröder, F.G., Sima, O., Toma, G., Trinchero, G.C., Ulrich, H., Weindl, A., Wochele, J., and Zabierowski, J., Cascade-grande: Composition studies in the view of the post-lhc hadronic interaction models, *EPJ Web Conf.* **145**, 13001 (2017).
 - [14] D. Bergman (Telescope Array), Telescope Array: Latest Results and Expansion Plans, *J. Phys. Conf. Ser.* **1468**, 012078 (2020).
 - [15] P. Abraham, J. and *et al*, Measurement of the energy spectrum of cosmic rays above 10^{18} eV using the Pierre Auger Observatory, *Physics Letters B* **685**, 239 (2010), arXiv:1002.1975 [astro-ph.HE].
 - [16] M. Nagano, M. Teshima, Y. Matsubara, H. Y. Dai, T. Hara, N. Hayashida, M. Honda, H. Ohoka, and S. Yoshida, Energy spectrum of primary cosmic rays above 10^{17} ev determined from the extensive air shower experiment at akeno, *Journal of Physics G: Nuclear and Particle Physics* **18**, 423 (1992).
 - [17] D. Allard, E. Parizot, A. V. Olinto, E. Khan, and S. Goriely, UHE nuclei propagation and the interpretation of the ankle in the cosmic-ray spectrum, *aap* **443**, L29 (2005), arXiv:astro-ph/0505566 [astro-ph].
 - [18] D. Allard, E. Parizot, and A. V. Olinto, On the transition from galactic to extragalactic cosmic-rays: Spectral and composition features from two opposite scenarios, *Astroparticle Physics* **27**, 61 (2007), arXiv:astro-ph/0512345 [astro-ph].
 - [19] V. S. Berezinskii and S. I. Grigor’eva, A bump in the ultra-high energy cosmic ray spectrum, *aap* **199**, 1 (1988).

- [20] V. Berezhinsky, A. Gazizov, and S. Grigorieva, On astrophysical solution to ultrahigh energy cosmic rays, *Phys. Rev. D* **74**, 043005 (2006), arXiv:hep-ph/0204357 [hep-ph].
- [21] R. Aloisio, V. Berezhinsky, and P. Blasi, Ultra high energy cosmic rays: implications of Auger data for source spectra and chemical composition, *JCAP* **2014**, 020 (2014), arXiv:1312.7459 [astro-ph.HE].
- [22] A. The Pierre Auger Collaboration, Aab and *et al*, The Pierre Auger Observatory: Contributions to the 36th International Cosmic Ray Conference (ICRC 2019), arXiv e-prints, arXiv:1909.09073 (2019), arXiv:1909.09073 [astro-ph.HE].
- [23] A. Aab and *et al* (The Pierre Auger Collaboration), Features of the energy spectrum of cosmic rays above 2.5×10^{18} eV using the pierre auger observatory, *Phys. Rev. Lett.* **125**, 121106 (2020).
- [24] A. di Matteo, , and *et al*, UHECR arrival directions in the latest data from the original Auger and TA surface detectors and nearby galaxies, *PoS ICRC2021*, 308 (2021).
- [25] J. Biteau, , and *et al*, The ultra-high-energy cosmic-ray sky above 32 EeV viewed from the Pierre Auger Observatory, *PoS ICRC2021*, 307 (2021).
- [26] R. U. Abbasi and *et al*, Indications of Intermediate-scale Anisotropy of Cosmic Rays with Energy Greater Than 57 EeV in the Northern Sky Measured with the Surface Detector of the Telescope Array Experiment, *apjl* **790**, L21 (2014), arXiv:1404.5890 [astro-ph.HE].
- [27] R. U. Abbasi and *et al*, Evidence for a Supergalactic Structure of Magnetic Deflection Multiplets of Ultra-high-energy Cosmic Rays, *apj* **899**, 86 (2020).
- [28] R. Jansson and G. R. Farrar, The Galactic Magnetic Field, *apjl* **761**, L11 (2012), arXiv:1210.7820 [astro-ph.GA].
- [29] A. Tritsis, C. Federrath, and V. Pavlidou, Magnetic Field Tomography in Two Clouds toward Ursa Major Using H I Fibers, *apj* **873**, 38 (2019), arXiv:1810.00231 [astro-ph.GA].
- [30] J. L. Puget, F. W. Stecker, and J. H. Bredekamp, Photonuclear interactions of ultrahigh energy cosmic rays and their astrophysical consequences., *apj* **205**, 638 (1976).
- [31] F. W. Stecker and M. H. Salamon, Photodisintegration of ultrahigh-energy cosmic rays: A New determination, *Astrophys. J.* **512**, 521 (1999), arXiv:astro-ph/9808110.
- [32] N. Shaham and T. Piran, Implications of the penetration depth of ultrahigh-energy cosmic rays on physics at 100 tev, *Phys. Rev. Lett.* **110**, 021101 (2013).
- [33] A. Aab and *et al* (Pierre Auger Collaboration*), Depth of maximum of air-shower profiles at the pierre auger observatory. ii. composition implications, *Phys. Rev. D* **90**, 122006 (2014).
- [34] A. Aab and *et al*, Combined fit of spectrum and composition data as measured by the Pierre Auger Observatory, *JCAP* **2017**, 038 (2017), arXiv:1612.07155 [astro-ph.HE].
- [35] N. Arsene, Mass Composition of UHECRs from Xmax Distributions Recorded by the Pierre Auger and Telescope Array Observatories, *Universe* **7**, 321 (2021), arXiv:2109.03626 [hep-ph].
- [36] T. Guido, E. and *et al*, Combined fit of the energy spectrum and mass composition across the ankle with the data measured at the Pierre Auger Observatory, in *37th International Cosmic Ray Conference. 12-23 July 2021. Berlin* (2022) p. 311.
- [37] M. Unger, G. R. Farrar, and L. A. Anchordoqui, Origin of the ankle in the ultrahigh energy cosmic ray spectrum, and of the extragalactic protons below it, *Phys. Rev. D* **92**, 123001 (2015).
- [38] N. Globus, D. Allard, and E. Parizot, A complete model of the cosmic ray spectrum and composition across the galactic to extragalactic transition, *Phys. Rev. D* **92**, 021302 (2015).
- [39] F. A. Sánchez, The muon component of extensive air showers above 10(17.5) eV measured with the Pierre Auger Observatory, in *36th International Cosmic Ray Conference (ICRC2019)*, International Cosmic Ray Conference, Vol. 36 (2019) p. 411.
- [40] A. Aab and *et al* (Pierre Auger Collaboration), Testing hadronic interactions at ultrahigh energies with air showers measured by the pierre auger observatory, *Phys. Rev. Lett.* **117**, 192001 (2016).
- [41] D. Veberic, ed., *The Pierre Auger Observatory: Contributions to the 35th International Cosmic Ray Conference (ICRC 2017)* (2017) arXiv:1708.06592 [astro-ph.HE].
- [42] A. Aab *et al*. (Pierre Auger), An Indication of anisotropy in arrival directions of ultra-high-energy cosmic rays through comparison to the flux pattern of extragalactic gamma-ray sources, *Astrophys. J. Lett.* **853**, L29 (2018), arXiv:1801.06160 [astro-ph.HE].
- [43] G. R. Farrar and J. D. Allen, A new physical phenomenon in ultra-high energy collisions, *EPJ Web Conf.* **53**, 07007 (2013), arXiv:1307.2322 [hep-ph].
- [44] L. A. Anchordoqui, H. Goldberg, and T. J. Weiler, Strange fireball as an explanation of the muon excess in auger data, *Phys. Rev. D* **95**, 063005 (2017).
- [45] G. Tomar, Lorentz invariance violation as an explanation of the muon excess in auger data, *Phys. Rev. D* **95**, 095035 (2017).
- [46] V. Pavlidou and T. Tomaras, What do the highest-energy cosmic-ray data suggest about possible new physics around 50 TeV?, *Phys. Rev. D* **99**, 123016 (2019), arXiv:1802.04806 [astro-ph.HE].
- [47] D. Heck, J. Knapp, J. N. Capdevielle, G. Schatz, and T. Thouw, *CORSIKA: a Monte Carlo code to simulate extensive air showers*. (1998).
- [48] T. Pierog, I. Karpenko, J. M. Katzy, E. Yatsenko, and K. Werner, Epos lhc: Test of collective hadronization with data measured at the cern large hadron collider, *Physical Review C* **92**, 10.1103/physrevc.92.034906 (2015).
- [49] S. Ostapchenko, Monte carlo treatment of hadronic interactions in enhanced pomeron scheme: Qgsjet-ii model, *Phys. Rev. D* **83**, 014018 (2011).
- [50] A. Ferrari, P. R. Sala, M. /CERN /INFN, A. Fasso, /SLAC, J. Ranft, and S. U., Fluka: A multi-particle transport code 10.2172/877507 (2005).
- [51] R. Ulrich, R. Engel, and M. Unger, Hadronic Multiparticle Production at Ultra-High Energies and Extensive Air Showers, *Phys. Rev. D* **83**, 054026 (2011), arXiv:1010.4310 [hep-ph].
- [52] B. Mohanty and J. Serreau, Disoriented chiral condensate: Theory and experiment [review article], *physrep* **414**, 263 (2005), arXiv:hep-ph/0504154 [hep-ph].
- [53] A. Cafarella, C. Corianò, and T. N. Tomaras, Cosmic ray signals from mini black holes in models with extra dimensions: an analytical/Monte Carlo study, *Journal of High Energy Physics* **2005**, 065 (2005), arXiv:hep-ph/0410358 [hep-ph].

- [54] A. Mironov, A. Morozov, and T. N. Tomaras, Can Centauros or Chirons BE the First Observations of Evaporating Mini Black Holes?, *International Journal of Modern Physics A* **24**, 4097 (2009), arXiv:hep-ph/0311318 [hep-ph].
- [55] C. Patrignani *et al.* (Particle Data Group), Review of Particle Physics, *Chin. Phys. C* **40**, 100001 (2016).
- [56] W. Heitler, *The quantum theory of radiation*, International Series of Monographs on Physics, Vol. 5 (Oxford University Press, Oxford, 1936).
- [57] J. Matthews, A heitler model of extensive air showers, *Astroparticle Physics* **22**, 387 (2005).
- [58] A. Aab *et al.* (Pierre Auger), Muons in Air Showers at the Pierre Auger Observatory: Mean Number in Highly Inclined Events, *Phys. Rev. D* **91**, 032003 (2015), [Erratum: *Phys.Rev.D* 91, 059901 (2015)], arXiv:1408.1421 [astro-ph.HE].
- [59] T. Bergmann, R. Engel, D. Heck, N. N. Kalmykov, S. Ostapchenko, T. Pierog, T. Thouw, and K. Werner, One-dimensional Hybrid Approach to Extensive Air Shower Simulation, *Astropart. Phys.* **26**, 420 (2007), arXiv:astro-ph/0606564.
- [60] A. Aab *et al.* (Pierre Auger), Large-scale cosmic-ray anisotropies above 4 EeV measured by the Pierre Auger Observatory, *Astrophys. J.* **868**, 4 (2018), arXiv:1808.03579 [astro-ph.HE].
- [61] R. U. Abbasi *et al.* (Telescope Array), Search for Large-scale Anisotropy on Arrival Directions of Ultra-high-energy Cosmic Rays Observed with the Telescope Array Experiment, *Astrophys. J. Lett.* **898**, L28 (2020), arXiv:2007.00023 [astro-ph.HE].
- [62] H. Dembinski *et al.*, The Muon Puzzle in air showers and its connection to the LHC, *PoS ICRC2021*, 037 (2021).
- [63] K. Tassis, A. N. Ramaprakash, A. C. S. Readhead, S. B. Potter, I. K. Wehus, G. V. Panopoulou, D. Blinov, H. K. Eriksen, B. Hensley, A. Karakci, J. A. Kypriotakis, S. Maharana, E. Ntormousi, V. Pavlidou, T. J. Pearson, and R. Skalidis, PASIPHAE: A high-Galactic-latitude, high-accuracy optopolarimetric survey, arXiv e-prints, arXiv:1810.05652 (2018), arXiv:1810.05652 [astro-ph.IM].
- [64] A. Tritsis, C. Federrath, N. Schneider, and K. Tassis, A new method for probing magnetic field strengths from striations in the interstellar medium, *mnras* **481**, 5275 (2018), arXiv:1810.01559 [astro-ph.GA].
- [65] S. E. Clark and B. S. Hensley, Mapping the Magnetic Interstellar Medium in Three Dimensions over the Full Sky with Neutral Hydrogen, *apj* **887**, 136 (2019), arXiv:1909.11673 [astro-ph.GA].
- [66] R. Skalidis and K. Tassis, High-accuracy estimation of magnetic field strength in the interstellar medium from dust polarization, *aap* **647**, A186 (2021), arXiv:2010.15141 [astro-ph.GA].
- [67] R. Skalidis, J. Sternberg, J. R. Beattie, V. Pavlidou, and K. Tassis, Why take the square root? An assessment of interstellar magnetic field strength estimation methods, *aap* **656**, A118 (2021), arXiv:2109.10925 [astro-ph.GA].
- [68] G. Magkos and V. Pavlidou, Deflections of ultra-high energy cosmic rays by the Milky Way magnetic field: how well can they be corrected?, *jcap* **2019**, 004 (2019), arXiv:1802.03409 [astro-ph.HE].